Associative properties of rapeseed napin and pectin: Competition between liquid-liquid and liquid-solid phase separation

Chloé Amine, Adeline Boire, Alice Kermarrec, Denis Renard

Associative properties of rapeseed napin and pectin: competition between liquid-liquid and liquid-solid phase separation.

Chloé Amine, Adeline Boire, Alice Kermarrec & Denis Renard*

UR1268 Biopolymères Interactions Assemblages, INRA, 44300 Nantes, France

* Corresponding author: denis.renard@inra.fr

Abstract: We investigated the assembly of a plant protein, rapeseed napin (NAP), mixed with a plant polysaccharide, highly methylated pectin (PEC). The optimum pH for NAP/PEC interactions was found at pH 4.0 for which the charge difference between the two biopolymers is the highest~~, corresponding to the highest electrostatic contribution between the two biopolymers~~. Two types of phase transition were observed depending on pH and mixing ratios: liquid-solid and liquid-liquid phase separation. We showed that liquid-solid transition was favored by strong electrostatic attraction whereas liquid-liquid phase separation was promoted by weaker attraction. In addition, we highlighted a solid-to-liquid phase transition overtime for ratios with excess of proteins. We showed that polysaccharide charge neutralization was a requisite for the transition as no rearrangement was observed when residual charges remained. ~~We discuss the role of protein flexibility in this phenomenon as napin is predicted to be partially disordered.~~ The underlying mechanism leading to this transition remains to be explored. To the best of our knowledge, such solid-to-liquid transition has never been reported for protein-polysaccharide mixtures.

Keywords. Complex coacervation. Napin. Pectin. Phase transition. Droplets millifluidic.

I. Introduction

Complex coacervation is an associative liquid-liquid phase separation primarily driven by attractive electrostatics interactions between two oppositely charged polyelectrolytes. There have been intense research efforts over the years to better understand and control complex coacervation with various applications in pharmaceutical, biomedical, cosmetic or food industry (Schmitt & Turgeon, 2011; Turgeon, Schmitt, & Sanchez, 2007). In case of strong attraction, liquid-solid phase separation, also called precipitation, may occur (Comert, Malanowski, Azarikia, & Dubin, 2016). It is usually associated with undesirable impact during processes such as inhomogeneity and irreproducible kinetics (Comert & Dubin, 2017). Understanding the competition between the two mechanisms and identifying parameters leading to one or the other mechanism is essential in the further development of coacervation applications.

Liquid-liquid phase separation is a reversible mechanism leading to the formation of spherical droplets in equilibrium with a diluted phase. The liquid-like state of the dense phase is inferred from the spherical shape of phase separated domains as well as their ability to fuse into larger round-shaped objects. On contrary, liquid-solid transition is generally an irreversible phenomenon leading to amorphous solid phases of irregular shape. Depending on the scientific community, several designations are found for such solid phases: “aggregates” (Nigen, Croguennec, Renard, & Bouhallab, 2007; Tavares, Croguennec, Hamon, Carvalho, & Bouhallab, 2015), “flocs” (Anema & de Kruif, 2014; Thongkaew, Hinrichs, Gibis, & Weiss, 2015) or “precipitates” (Comert et al., 2016; Obermeyer, Mills, Dong, Flores, & Olsen, 2016). In the literature, the differentiation between the two mechanisms is often obscured by the common use of turbidity to detect such transitions (Comert & Dubin, 2017). Both mechanisms induce an increase in turbidity but microscopy is needed to know whether the turbidity arises from liquid-liquid or liquid-solid phase separation. Looking into turbidity kinetics may also help ~~in to~~ discriminate between the two phenomena (Chapeau et al., 2016). It is generally accepted that strong attractive properties favor liquid-solid phase separation. In a recent review, Comert and Dubin discussed the influence of several parameters favoring liquid-solid phase transition (Comert & Dubin, 2017). Charge anisotropy, due to "positive patches" on protein surface or a blockwise distribution of charged groups along the polyelectrolyte, is thought to promote liquid-solid phase separation. It induces high local charge density leading to local strong attraction despite low net charge (Mattison, Dubin, & Brittain, 1998). The polyelectrolyte pK_a also play a role on the formation of solid precipitates in protein-polyelectrolyte systems. In case of low pK_a, lowering the pH results in an increase in protein charge density while the charge density of the polyelectrolyte remains maximal due to complete charge dissociation. In this case, the electrostatic interaction are strong and may lead to liquid-solid phase transition as observed for polyvinyl sulfonic acid and

lysozyme (Romanini, Braia, Angarten, Loh, & Picó, 2007). The structure of the polyelectrolyte also modulates the type of phase separation observed. Coacervation is favored by branched polyelectrolyte (Comert et al., 2016) and flexible ones (Cousin, Gummel, Combet, & Boué, 2011; Kizilay, Kayitmazer, & Dubin, 2011).

Here, we aimed at investigating the interplay between liquid-liquid and liquid-solid phase separation in protein-polysaccharide mixtures. We investigated the electrostatic assembly of a basic protein, rapeseed napin (NAP), and an acidic polysaccharide, highly methylated pectin (PEC) known to form electrostatic complexes at pH 7 (Schmidt, 2004). Turbidity measurements, phase compositions determination and microscopy observations were performed. The assembly of NAP/PEC mixtures was assessed as a function of pH to tune NAP/PEC binding affinity and as a function of NAP/PEC ratio to tune complex charge. ~~We did so using turbidity measurement, phase compositions determination and microscopy.~~ We showed that liquid-solid phase separation is favored at low pH when the electrostatic attraction was the strongest. On contrary, liquid-liquid phase separation was favored at intermediate pH. More interestingly, a transition from solid-to-liquid was observed overtime at low pH in case of excess of protein suggesting that the liquid-solid phase separation is not always irreversible. We discuss the potential role of charge re-arrangement and protein intrinsic disorder~~flexibility~~ in this behaviour.

II. Materials and Methods

II.1. Materials

Napin was purified from defatted rapeseed meal using an adapted protocol already published (Schmidt et al., 2004). Defatted rapeseed meals were obtained at the pilot scale using CETIOM facilities (Pessac, France). Proteins were extracted from the meal in an extraction buffer (50 mM Tris, 1M NaCl, 15 mM sodium disulfite, 5 mM EDTA, pH 8.5) during 1 hour at room temperature. After centrifugation at 17 000 g during 20 minutes at 20°C, a second extraction was performed to recover most of soluble proteins. Supernatant were combined and filtered on a sintered filter (N°0). Pigments were removed by a size-exclusion chromatography on a Cellufine GH 25 column (Amicon, 100 x 887 mm, 7.5 L) equilibrated in buffer A (50 mM Tris, 5 mM EDTA, pH 8.5). Proteins were eluted with buffer A. Napins were then fractionated by ionic exchange chromatography using a SPsepharose fast flow column (Amersham XK50/15, 300 ml). The elution of napin was performed using an increasing gradient of buffer B (buffer A + 1 M NaCl). The eluted fractions were then extensively dialysed against water at 4°C and freeze dried. Napin was further purified by gel filtration on a sephadex G50

medium (Pharmacia , 1.8L) equilibrated in buffer C (50mM Tris, 0.75M NaCl, pH 8.5). Finally, the samples were dialyzed against water before freeze-drying.

The protein content of purified powder was higher than 95% on a dry basis, using the Dumas Method with a corrective factor of 5.5 (Mosse, 1990). Ash content was about 8.5 % using thermogravimetric analysis under nitrogen atmosphere. Napin powder was stored under vacuum at -20 °C until use. It was placed at 20 °C in a desiccator containing K_2CO_3 saturated salt during whole time of experiments to ensure constant moisture content. The purity of napin was checked by SDS-PAGE electrophoresis and mass spectrometry as presented in Supplementary data. Two major isoforms of napin were identified ascribed to 2SS3 and 2SS2, respectively. These results were in agreement with those previously described by Schmidt et al. (2004).

Highly methoxylated Pectin (UniPectin QC-100, batch number 47572901) provided by Cargill (France) was used with a degree of methylation of 71 % and a mean molecular weight of 227 kg mol^{-1}. A detailed characterisation is given in Supplementary data. Pectin powder was stored at room temperature during the whole time of experiments. A characterization study performed on individual biopolymer is given in Supplementary data (Figure S1).

Hydrochloric acid (HCl), sodium hydroxide (NaOH) and sunflower oil were supplied from Sigma. Bodipy TR Cadaverin dye (λ_{exc} 588 nm, λ_{em} 616 nm**,** D6251) and Alexa Fluor 350 NHS ester dye (λ_{exc} 346 nm, λ_{em} 442 nm**,** A10168) were provided by Thermoscientific. N-(3-Dimethylamino-propyl)-N'-ethyl-carbodiimide hydrochloride (EDC) and N-hydroxysuccinimide (NHS) used for pectin activation came from Sigma. Milli-Q water was used in all sample preparations.

II.2. Biopolymers stocks dispersions

Napin and Pectin powders were solubilized overnight at 20°C. The following buffers were used according to the pH: acetate buffer (10 mM) for pH 4.0 and pH 5.0; MES buffer (10 mM) and phosphate buffer (10 mM) for pH 6.0 and pH 7.0, respectively. The ionic strength (I) was adjusted to 25, 50, 75, or 150 mM using NaCl. The resulted biopolymers dispersions were then filtered on a 0.2 µm cellulose acetate membrane (Sartorius, France). The protein concentration was determined by UV absorption spectrophotometry at a wavelength of 278 nm using ε_{Napin}= 0.57 $L.g^{-1}.cm^{-1}$ (Schmidt, Renard, Rondeau, Richomme, Popineau, & Axelos, 2004) whereas polysaccharide concentration was obtained by dry matter analysis. Concentrations were adjusted in a range between 0.1 to 1 wt% by dilution in the buffer.

II.3. Biopolymers charge determination

II.3.1. Electrophoretic mobility

Electrophoretic mobility measurements were performed on biopolymers stock dispersions as a function of pH using a zetasizer Nano Series (Nano-ZS, malvern instrument). Experiments were conducted at 20°C in triplicate. Biopolymers were solubilised overnight at 0.25 wt% in Milli-Q water under magnetic stirring before being filtered on 0.2 µm cellulose acetate membrane (Sartorius). The pH of the dispersions was adjusted in a range between 3.0 and 11.0 with HCl or NaOH 0.2M before experiments.. Similarly, measurements were performed on biopolymers mixtures at pH 4.0, 0.5 wt% total concentrations for several NAP/PEC mixing ratios ranging from 1:8 to 16:1.

II.3.2. Potentiometric titration

Biopolymers surface charge evolution with pH was obtained by potentiometric titration as described previously (Salis et al., 2011) using an automated titranto 905 (Methrom, France). Biopolymer solutions (0.1 wt%) in Milli-Q water, filtered through 0.2 µm (cellulose acetate, Sartorius) was pre-titrated by HCl 10^{-2} M to reach a pH equal to 2.5. The resulted acidic dispersions was then titrated to pH 11 using NaOH 10^{-2} M. Pre-titration and titrations were performed in the same conditions as a blank solution made of milli-Q water. The biopolymer surface charge Z_p was finally calculated as a function of pH using the following equation:

$$\mathrm{Zp} = \frac{[HCl](V_{HCl} - V_{HCl\,blank}) - [NaOH](V_{NaOH} - V_{NaOH\,blank})}{m_{biop}/M_{biop}}$$

where V_{HCl} is the volume (mL) of HCl used in the pre-titration to reach pH 2.5 for the sample and the blank. V_{NaOH} is the volume of NaOH used in the titration of both sample and blank. m_{biop} (g) is the mass of biopolymer introduced in the sample and M_{biop} (g/mol) is the molecular weight of the biopolymers. [HCl] and [NaOH] are the molar concentration (mol/L) of hydrochloric acid and sodium hydroxide used during pre-titration and titration experiments.

II.4. Screening of NAP/PEC interactions using microplates

The screening of NAP/PEC interactions was performed at 0.1 wt% total biopolymers concentration using an Automated Laboratory Microplates handling (Biomek 3 000, France) combined with a shaker (Variomag Teleshake, Thermofischer). Experiments were conducted in a 20°C regulated room. The impact of pH (4.0, 5.0, 6.0 and 7.0) and NAP/PEC mixing ratio (8:1, 4:1, 3:2, 2:3, 1:4 and 1:8) was investigated. The equivalence between initial NAP/PEC mixing ratio and the percentage of napin in the mixture was given in Table 1. Note that ionic strength was set to 25 mM for all pH values.

Mixtures were generated directly in a polystyrene 96 well microplates with flat bottom (651101, Greiner bio one, France). The volume of each well was set at 200 µL. The filling of microplates was performed as follows. First, wells were filled with napin stock dispersion prepared at 0.5 wt%. Then, protein was diluted by addition of buffer. Finally, pectin solution at 0.5 wt% was added. Shaking steps after buffer and pectin addition ensured the mixing. The time required for one 96 well microplate preparation was about 100 min. The time t_0 used in the following will referred to the time required to generate the 96 biopolymers mixtures, *i.e*, after pectin was added in the first well: this time was about 60 min. The impact of pH and mixing ratio on NAP/PEC interactions was assessed through turbidity measurements: the absorbance was recorded at a wavelength of 600 nm using a Microplates spectrophotometer (Biotek Epoch Microplate Spectrophotometer, France). Measurements were performed immediately after microplate generation (t_0) and once a day during one week. Microplates were stored at 20 °C during experimental time. Absorbance was converted into turbidity (τ, cm^{-1}) using the following equation: $\tau = (2.303 \times A_{600}) / l$, where l is the light path length (cm). l, equal to 0.6 cm, was calculated according to the following equation: $l = (4V/\pi d^2)$. After one week, NAP/PEC assemblies were also observed directly within the microplate using an inverted phase contrast optical microscope (BX51, Olympus, Germany) set at the magnification x 40.

II.5. Droplets based millifluidic for NAP/PEC screening of interactions

II.5.1. Millifluidic set-up

Millifluidic was shown to be an efficient and low material consuming approach to screen biopolymers interactions at total concentrations higher than 0.1 wt% (Amine, Boire, Davy, Marquis, & Renard, 2017). The developed experimental set-up, presented in Figure 1A is made of 4 modular parts. First, droplets generation in a sunflower oil continuous phase was ensured by a co-flow geometry comprising three inlets: two for the biopolymers dispersed phases and one for the oil continuous phase (Figure 1B). Two 2.5 mL glass syringes (Hamilton) respectively filled with NAP and PEC dispersions were placed on a syringe pump (Harvard Apparatus PHD 2000, France). A T-junction (ID 0.25 mm, Upchurch Scientific®) connected to the initial stocks dispersions through FEP tubes (interior diameter (ID) 0.51 mm, outside diameter (OD) 1.57 mm, length (L) 40 cm) ensured the mixing of the two components. The resulting mixture went through a fused silica capillary tube (ID 0.7 mm, OD 0.85 mm, L 12.5 cm) at a total flow rate of 3 mL / h. The continuous oil phase was pumped through a FEP tube (ID 0.51 mm, OD 1.57 mm L 40 cm) at a flow rate of 10 mL / h. Droplets of about 1.9 µL, displaying same size, shape and compositions, were finally generated into a transparent Tygon® tube (ID 1.42 mm, OD 3mm, L 55 cm). After generation, droplets went through a winding Tygon® tube (L 30 cm) which ensured the complete mixing within droplets based on chaotic advection (Song, Tice,

& Ismagilov, 2003) (Figure 1C). Droplets then reached a straight Tygon® tube (L 15 cm) placed on a PDMS support filled with ethylene glycol. This allowed on-line droplets observations 5 min after mixture generation (Figure 1D). Finally, an additional detachable module for long time droplets storage was connected to the device. The Tygon® tube containing droplets was connected to a multi junction made of PDMS. This allowed a convenient and rapid storage of 9 mixing conditions in a second PDMS support filled with ethylene glycol (Figure 1E). The use of slide clamps placed on the tubes (Word Precision Instruments, France) allowed a successive filling of each tube. Tubes were finally disconnected from the millifluidic device for longer storage and observed as a function of time directly within the PDMS support containing ethylene glycol.

Preliminary interfacial tension measurements confirmed that in the chosen range of concentrations, the percentage of adsorbed protein at the interface was negligible compared to the initial bulk concentration (see Supplementary data, Figure S2).

II.5.2. Optical set-up for droplets observations

Biopolymers droplets observations were carried out under continuous flow, directly within the Tygon® tube immersed in an ethylene glycol bath designed with PDMS. The light source was composed of 12 green LED (Radiospares, France) and arranged to obtain a dark field image on the camera. Pictures were taken at a distance of 155 mm from the Tygon tube using an objective with a fixed 1.5x magnification (OPT-043-216310, Alliance Vision). The objective was connected to a 7x manual zoom (OPT-043-300098, Alliance Vision), a TV-tube (OPT-001 0.67x, D 35 mm, L 117.7 mm, Alliance Vision) and a camera (SVS-ECO674MTLGEC, GigE, 2/3'' C'', 1920x2460, Alliance Vision, France) (Figure 1A). 10 pictures (1 droplet per pictures) were taken. A MatLab procedure was finally used to determine the average grey level. The analysis was done on a circular section of each droplet corresponding to about 75-80 % of the total area. Grey levels were converted into turbidity using a calibration based on TiO_2 dispersions as detailed previously (Amine et al., 2017).

II.5.3. Screening of NAP/PEC interactions by droplets-based millifluidic

Experiments were performed at pH 4.0 in acetate buffer (10mM, ionic strength of 25 mM) and room temperature. The impact of total biopolymers concentrations from 0.1 to 1 wt %, and Pr:Ps mixing ratio from 1:8 to 8:1 on droplets grey level were investigated. Mixing ratio was tuned by flow rates variation. Between two ratios, an equilibrium time of 80 s was applied to reach the desired composition. Droplets at the desired composition were finally generated during 35 s, analysed on-

line, and stored over two days in the PDMS support. Observations were also performed after 24 h and 48 h.

II.6. Determination of phases composition at thermodynamic equilibrium

Phases composition of biopolymers mixtures was determined for the following mixing ratios: 2:3, 1:1, 3:2, 4:1 and 8:1 at 0.5 wt% in 10 mM acetate buffer (pH 4.0, ionic strength of 25 mM). NAP/PEC mixtures were prepared into 1 mL conical bottom-sealed pipette tip and the volume was set at 300 µL for each condition. The amounts of napin and pectin used for mixtures preparation were accurately weighted to deduce the exact initial compositions. Mixtures were equilibrated 48 h in a 20 °C regulated room, before being centrifuged 1 h at 10 000 g. The supernatant, corresponding to the dilute phase was then collected using micropipette. Napin content in the dilute phase was obtained by UV absorption spectrophotometry at a wavelength λ of 278 nm. Pectin content was determined by the automated MHDP method (Thibault, 1979). Conical bottom-sealed pipette tips containing the coacervate phase were weighted and coacervate phase composition was deduced using mass conservation equation. This gravimetric approach gave an estimation of NAP and PEC contents in pellets with an accuracy of about +/-5 %.

II.7. Microscopy

II.7.1. Phase contrast microscopy

Biopolymers mixtures were observed as a function of time using a phase contrast optical microscope (BX51, Olympus, Germany) set at the magnification x 40 to evidence the presence or absence of coacervates. Observations were carried out on a glass microscope slide with a geneframe® (Thermo scientific).

III. Results & discussion

III.1. Napin and pectin carry opposite charges in a wide range of pH

Electrophoretic mobility was determined as a function of pH to identify conditions where napin and pectin carry opposite charges. Under acidic conditions, napin electrophoretic mobility is positive and decreases to reach 0 at a pH of 9.5 as reported in Figure 2. This pH value corresponds to the isoelectric point (IEP) of napin in agreement with literature data (Ericson et al., 1986; Gehrig, Krzyzaniak, Barciszewski, & Biemann, 1996; Josefsson, Lenman, Ericson, & Rask, 1987; Monsalve & Rodriguez, 1990). For higher pH, electrophoretic mobility is negative. Electrophoretic mobilities of

pectin are negative over the entire range of pH and reach a plateau value above pH 6.0 meaning all carboxylic functions are deprotonated. These negative values are in accordance with the pK_a of 2.8-3 previously determined for pectin (Ralet, Dronnet, Buchholt, & Thibault, 2001). These results suggest that electrostatic assembly between napin and pectin can take place over a wide pH range between 3.0 and 9.5.

III.2 NAP/PEC assemblies are maximal for the highest charge difference

We intended to identify NAP/PEC assembly conditions using turbidity measurements as a function of pH, in a range where biopolymers carry opposite charges. Turbidity increases for decreasing pH, being the highest at pH 4.0 (Figure 3~~A~~). This pH corresponds to a point where the overall charge difference between biopolymers is maximal as seen in Figure 2. Increasing pH from 4.0 to 7.0 induces a decrease in the overall charge difference between biopolymers. The electrostatic attraction ~~contribution~~ between napin and pectin is therefore expected to be maximal at pH 4.0. pH 4.0 also corresponds to the pH of electrical equivalence (EEP) defined as the pH where biopolymers carried equal and opposite charges (Burgess & Carless, 1984). ~~In this case, the overall charge balance reaches 0 as plotted in Figure 3B.~~ The formation of NAP/PEC assemblies, maximal at pH 4.0 and characterized by high turbidity, is therefore primarily driven by long-range electrostatics interactions which is consistent with protein-polysaccharide complex coacervation (de Kruif, Weinbreck, & de Vries, 2004).

Protein:Polysaccharide (Pr:Ps) mixing ratio is another important parameter in mixed biopolymers systems. It controls biopolymers charge balance while keeping the binding affinity constant (Antonov, Mazzawi, & Dubin, 2010; Xia & Dubin, 1994). Low NAP/PEC mixing ratio (protein content lower than 20%) is associated to low turbidity, suggesting no macroscopic phase separation in the entire pH range investigated (Figure 3~~A~~). In these cases, the number of protein molecules in the solution may not be sufficient to neutralise the negative charges of all pectin molecules. It is a common result already observed in the literature and has been ascribed to a negative residual net charge of the complexes which remain soluble (Zaitsev, Izumrudov, & Zezin, 1992). As NAP/PEC mixing ratio increases, the higher protein content may lead to the neutralization of polysaccharide charges inducing macroscopic phase separation. A sharp increase in turbidity is indeed observed at pH 4.0, with a maximum for a NAP/PEC mixing ratio of 3:2.

The optimum NAP/PEC mixing ratio for NAP/PEC assemblies, defined as the highest turbidity, is pH dependent and shifts towards higher NAP/PEC mixing ratio for increasing pH. At high pH values, close to napin IEP, a decrease in surface charge ~~density~~ and electrophoretic mobility is observed. On the contrary, pectin surface charge ~~density~~ and electrophoretic mobility remain constant, in view of

complete deprotonation of carboxylic groups. Therefore, more napin molecules are required to compensate pectin negative charges. As NAP/PEC assembly is maximal at pH 4, further experiments were conducted at this pH.

III.2. NAP/PEC phase separates into associative assemblies independently of total concentration.

Associative phase separation and complex coacervation usually occurs in a restricted range of concentration (Veis, Bodor, & Mussell, 1967). We assessed the role of total biopolymers concentration on NAP/PEC assemblies using droplets based millifluidic to limit material consumption (Amine et al., 2017). Experiments were conducted at pH 4.0 for concentrations ranging from 0.1 to 1 wt%. The high pectin viscosity as well as its high intrinsic turbidity prevented to work at higher pectin concentration. The evolution of droplets grey level obtained from image analysis is presented in Figure 4A as a function of NAP/PEC mixing ratio. In the studied range of concentrations, pure napin and pure pectin are limpid. Turbidity profiles follow a similar trend regardless of total biopolymers concentration. Droplets are limpid at low NAP/PEC mixing ratio (1:8, 1:4) meaning that no macroscopic phase separation occurred. This was confirmed by optical microscopy observations of millifluidic droplets, where no supramolecular assemblies were detected (data not shown). At these NAP/PEC ratio, small complexes probably form. Further experiments like dynamic light scattering should be performed to probe their size and kinetics of formation. The maximum of interaction is comprised between a ratio of 1:1 and 3:2 according to the total biopolymers concentration. However, for these two ratios, the turbidity of droplets is heterogeneous as shown in Figure 4B. The heterogeneity is more pronounced at high concentrations. It is not possible to conclude whether the difference in grey level between ratios 1:1 and 3:2 was significant or not. For total biopolymers concentrations ranging from 0.1 to 1 wt%, NAP/PEC interaction profile is thus similar. In this range of concentration, phase separation profile does not depend on concentration. The increase in grey level with total biopolymers concentration at fixed Pr:Ps mixing ratio is assigned to an increase in dense lower phase volume fraction. This behaviour was previously evidenced on BSA/PDMDAAC mixtures where no effect of total solute concentration on the phase boundary was detected (Mattison, Brittain, & Dubin, 1995). Considering pectin/gelatin mixtures, McMullen et al. highlighted an optimum total biopolymers concentration of 2% for coacervation (McMullen, Newton, & Becker, 1982). Above this value, coacervation yield decreased. Self-suppression of NAP/PEC interactions may also occur but high viscosity of pectin above 1 wt% prevented to perform efficient mixing of the biopolymers using a T-junction in droplets millifluidic. In addition, turbidity assigned to pectin self-aggregation at high pectin concentration excluded a clear interpretation of any increase of turbidity.

Phase composition was determined at thermodynamic equilibrium at a total concentration of 0.5 wt%. It provides additional information as compared to turbidity measurement: the phase separation yield. The maximum of phase separation yield was obtained for a mixing ratio of 3:2, where 83% of the initial quantity of biopolymers was in the dense lower phase (Figure 4D). For a mixing ratio of 1:1, the yield of phase separation is equal to 75%. These results are well correlated with the high turbidity probed using droplets based millifluidic for these two mixing ratios. From these complementary results, NAP/PEC phase diagram at pH 4.0 is plotted in Figure 4C. Note that additional conditions close to the initiation of phase separation should be investigated to have a more precise idea of the position of the coexistence curve. In addition, the detailed napin and pectin compositions at thermodynamic equilibrium are given in supplementary data (see Supplementary data, Figure S3). Both biopolymers are enriched in the dense phase confirming an associative phase separation. The co-localization of both biopolymers within assemblies was further confirmed using confocal laser scanning microscopy (see Supplementary data, Figure S4).

III.3. Charge neutralisation controls the structure of NAP/PEC assembly

The structure of NAP/PEC assemblies was assessed using phase contrast microscopy. Observations were performed over time (1h) on mixtures with different mixing ratios inducing macroscopic phase separation (8:1, 4:1, 3:2, 1:1, 2:3). Two types of structures are evidenced by phase contrast microscopy according to observation time and mixing ratio: coacervates and solid-like structures as shown in Figure 5. When protein is in excess in the initial solution, *i.e* mixing ratio of 8:1, 4:1 and 3:2, a coexistence of these two structures is observed immediately after biopolymers mixing (2min). Coacervates droplets size and number increase over time (15 and 60 min after biopolymers mixing). The size of the unshaped solid-like structures, which displayed high similarities with solid precipitates (Comert & Dubin, 2017; Kayitmazer, Koksal, & Iyilik, 2015), increases as mixing ratio decreased. Interestingly, the solid-like structures rearrange over time and form after 1 h large liquid-like structures. It suggests a solid-to-liquid transition occurring over time at these three mixing ratios. Microscopy experiments performed on several supports, glass slide, microplate and low binding microplate, led to similar observations, confirming that solid-to-liquid transition was not due to surface effects (data not shown). When protein content within mixtures is further decreased (NAP/PEC mixing ratio of 1:1 and 2:3), only solid-like structures are visible. Despite an increase in structures density with time, the characteristic size does not increase. We therefore evidenced two types of NAP/PEC assembly depending on both mixing ratio and time: liquid droplets and solid-like structures being predominant in the system.

To better understand factors underlying these structural differences according to Pr:Ps mixing ratio, the charge of mixtures was determined by measuring the electrophoretic mobility μ_E. Two regimes of mobility can be observed as a function of the initial mixing ratio as displayed in Figure 6. In conditions where solid-like structures are formed (NAP/PEC ratio from 1:8 to 1:1) a highly negative μ_E is obtained which depends weakly on initial mixing ratio and is very similar to pectin mobility. This suggests that pectin is the main contributor to the electrophoretic mobility. ~~An excess of negatively charged pectin macromolecules might stabilize the assemblies and prevent coalescence to occur. This could explain the smaller size of NAP/PEC assemblies observed at these ratios.~~ In contrast, a μ_E close to 0 is obtained in conditions where rearrangement over time is observed (NAP/PEC ratio from 3:2 to 8:1). ~~Charge neutralisation is a requisite for spherical coacervate droplets formation that can be subjected to coalescence phenomenon.~~ The measurement of an electrophoretic mobility on multiphasic dispersions is however questionable as it gives an average value of multiple species present in dispersions such as free biopolymers, soluble and insoluble complexes and coacervates.

An alternative method can be used to evaluate the charge of NAP/PEC assemblies. It consists in determining each biopolymer charge using potentiometric titration and calculating theoretical charges of the assemblies based on composition. The evolution of the number of charge per mol of biopolymer, Z_p/M_w, as a function of pH was determined for both napin and pectin as shown on Figure 7A. Highly similar profiles were obtained when compared to electrophoretic mobility measurements presented on Figure 2. The point where napin carried 0 charges is around pH 9.5 whereas pectin is completely deprotonated above pH 6 as evidenced by the plateau value. Additionally, experimental data obtained for napin are very similar to those calculated using the Uniprot calculator software with napin sequence 2SS3. At pH 4, one napin molecule carries 14 positive charges whereas each pectin molecule carries 160 negative charges. From the knowledge of each biopolymer charge at pH 4 and from phase compositions obtained at thermodynamic equilibrium, Pr/Ps [+]/[-] charge ratio in the dense lower phase was evaluated as a function of initial mixture composition (Figure 7B). Pr/Ps [+]/[-] charge ratio in the dense lower phase is highly dependent on the initial weight mixing ratio: the higher the initial Pr:Ps weight mixing ratio is, the higher the Pr/Ps [+]/[-] charge ratio in the dense lower phase is. This indicates an increase in protein content within the lower phase. This trend has been previously reported for other protein-polysaccharide mixtures (Comert et al., 2016; de Kruif et al., 2004; Schmitt, Sanchez, Thomas, & Hardy, 1999; Sanchez et al., 2002; Pathak, Priyadarshini, Rawat, & Bohidar, 2017; Niu et al., 2015; Sperber, Schols, Cohen Stuart, Norde, & Voragen, 2009; Wee et al., 2014; Niu et al., 2014; Vinayahan, Williams, & Phillips, 2010) and was ascribed to a mass action phenomenon. As the initial protein concentration increases, more protein molecules are involved in phase separation. At high Pr:Ps weight mixing ratios (4:1 and 8:1), where solid to liquid transition is observed, charge compensation is not reached (Pr/Ps [+]/[-] charge ratio not equal to 1)

and corresponds to the highest charge asymmetry. This result contradicts the measured μ_E which equals 0 for these Pr:Ps ratios (see Fig. 6). It is therefore difficult to conclude whether coacervation occurs at charge neutrality. The composition of the complexes could be different from the weight mixing and charge ratios due to charge regularization. This assumption could therefore justify the discrepancies observed between mobility measurements on complexes and calculated charge ratio from phase composition. Similar discrepancies were observed in the complex coacervation process between lactotransferrin and β-lactoglobulin (Anema & de Kruif, 2014). The calculated mixing charge ratio was systematically lower than the mixing ratio at zero zeta potential whatever the pH. In another study dealing with the complex coacervation between lactoferrin and caseins, the same authors also highlighted the existence of charged coacervates for mixing ratios far away from the optimum mixing fraction (Anema & de Kruif, 2016). In another study dealing with polysaccharide (hyaluronic acid) - polysaccharide (chitosan) complex coacervation, coacervate suspensions were also still observed with zeta potential values much higher than zero (Kayitmazer et al., 2015). This non-stoichiometric coacervation was explained by the fact that some interpolymer complexes assumed net charges further from neutrality in order for others to attain it (disproportionation theory), pK_a shifts within the system due to charge-charge interactions, partial loss of configurational entropy arising from the flexibility of polysaccharides, and "mismatch" (inequivalence) in charge spacing of the polysaccharide chains.

III.4. NAP/PEC aggregation is promoted by high electrostatic attraction

It has been previously suggested that liquid-solid phase separation is favoured for strong electrostatic attraction (Comert & Dubin, 2017). To check whether the liquid-solid phase separation of NAP/PEC was controlled by the charge difference between biopolymers, mixtures at a fixed NAP/PEC ratio of 8:1 were prepared at pH ranging from 4.0 to 9.0. Increasing pH from 4.0 to 9.0 leads to a decrease in napin positive charges as it approached its IEP (9.5) whereas pectin negative charges reaches a plateau value above pH 6.0 (Figure 2A). Increasing pH from 4.0 to 9.0 leads therefore to a decrease in initial charge ratio [+]/[-] between biopolymers from 11.9 to 1.4. Micrographs obtained after 1h by phase contrast microscopy are presented in Figure 8. Regardless of pH, a mixing ratio of 8:1 leads to the formation of coacervates droplets. However, an increase in pH induces a decrease in droplets size which appears also much more homogeneous in size. The suppression of large solid-like structures above pH 5 is attributed to the decrease in initial NAP/PEC charge ratio and consequently attractive electrostatic forces. Liquid-solid phase separation in NAP/PEC mixtures is indeed driven by strong electrostatic attraction.

Strong electrostatic attraction is however not sufficient to promote liquid-solid transition. The flexibility of biopolymers also plays a crucial role (Pathak et al., 2017). We investigated the assembly of napin with the major fraction of Acacia gum isolated by hydrophobic interaction chromatography, HIC-F1, and characterized elsewhere (Renard et al. 2006; Sanchez et al. 2008). HIC-F1 is a hyperbranched arabinogalactan-peptide characterized by a molecular weight and an electrophoretic mobility similar to HM-pectin in our buffer conditions. Their persistence length is however different: about 3 nm for HIC-F1 (Sanchez et al., 2008) and 8 nm for pectin (Schmidt et al., 2009). At pH 4.0, high turbidity was observed in NAP/HIC-F1 mixtures for mixing ratios comprised between 2:3 and 8:1 (Figure 9A). This high turbidity suggests strong associative properties and it was always associated with spherical droplets as displayed in Figure 9B. It can therefore be concluded that only liquid-liquid phase separation occurs when napin is mixed with a more flexible biopolymer such as HIC-F1.

III.VI. Deciphering the driving force of solid-to-liquid transition

For specific conditions where protein was in large excess in the initial mixture (ratio 8:1 to 3:2) a transition from solid-like to liquid-like droplets phase was observed in time. In these conditions, polysaccharide charges are probably neutralised by the excess of proteins. Residual interactions between NAP/PEC may play a key role in the re-arrangement over time. Time-dependent coacervation has been observed for gelatin A – gelatin B mixtures. The size of soluble intermolecular solid-like structures in the supernatant increased with time and was ascribed to residual electrostatic interactions (Tiwari, Bindal, & Bohidar, 2009). However, no microscopy observations clearly identified solid-to-liquid transition for gelatin A – gelatin B. A solid-to-liquid transition has been previously evidenced for apo α-lactalbumin/lysozyme mixture upon increasing temperature. It has been ascribed to an increased flexibility of apo α-lactalbumin due to its thermal denaturation (Nigen et al., 2007). Interestingly, previous NMR study reported the existence of several disordered loops in the tertiary structure of napin (Rico et al., 1996). The resulting 3D-structure displays disordered regions as highlighted by arrows in Figure 10A. In addition, napin disordered regions are hydrophilic as given by the hydropathy index in Figure 10B. As flexibility and hydration are interconnected parameters, they could contribute to the solid-to-liquid transition experimentally observed. The underlying mechanism is however not clear yet and deserve further investigations. As the solid-to-liquid transition occurs in excess of protein, a competition between protein-protein and protein-polysaccharide interactions may also occur. We checked the aggregation state of napin in our

experimental conditions using dynamic light scattering and found an hydrodynamic radius of 2.0 nm (data not shown), value in agreement with previously reported data (Schmidt et al., 2004). The initial aggregation state of napin is therefore not involved in the re-arrangement. However, it cannot be excluded that protein-protein interactions occur in the condensed coacervate-like phase as concentrations are higher than 200 g/L. This issue would need to be investigated in a future work.

Conclusion

In the current study, the electrostatic assembly of NAP/PEC was investigated in a pH range where biopolymers carry opposite net charges. Conditions of interactions were screened as a function of pH and mixing ratio to tune biopolymer binding affinity and complexes charge. The formation of NAP/PEC electrostatic assemblies was found to be maximal at pH 4.0. Up to 1 wt%, no impact of total biopolymers concentration was evidenced on phase separation conditions. However, the type of mechanism involved, liquid-liquid and liquid-solid phase separation, was strongly dependent on pH and initial NAP/PEC mixing ratio. Strong electrostatic interactions promoted by low pH led to liquid-solid phase separation whereas liquid-liquid phase separation was favoured for weaker attraction. However, for a given interaction potential, we showed that the NAP/PEC ratio also affected the type of phase separation mechanism. In case of excess of proteins, a reorganization of solid-like amorphous structures into liquid-like droplets phase was observed in time. This kinetically-driven phase transition could be promoted by residual interactions between biopolymers and/or protein conformation.

Acknowledgments

The authors acknowledge Joëlle Davy and Patrice Papineau for their strong technical support for designing the millifluidic device and Anne-Laure Reguerre for the image analysis. Marie-Jeanne Crépeau is thanked for her technical support on the automated Orcinol method, Véronique Solé-Jamault for her help with protein purification, Elisabeth David-Briand for her technical assistance for interfacial tension measurements, Thierry Doco, Pascale Williams and Michael Nigen for the biochemical and molecular characterization of pectin. This work was carried out with the financial support of the French Agronomic Research National Institute (INRA) and the Region Pays de la Loire.

References

Amine, C., Boire, A., Davy, J., Marquis, M., & Renard, D. (2017). Droplets-based millifluidic for the rapid determination of biopolymers phase diagrams. *Food Hydrocolloids*, 70, 134-142. http://doi.org/10.1016/j.foodhyd.2017.03.035

Anema, S. G., & de Kruif, C. G. (2016). Phase separation and composition of coacervates of lactoferrin and caseins. *Food Hydrocolloids*, *52*, 670–677. http://doi.org/10.1016/J.FOODHYD.2015.08.011

Anema, S. G., & de Kruif, C. G. (Kees). (2014). Complex coacervates of lactotransferrin and β-lactoglobulin. *Journal of Colloid and Interface Science*, *430*, 214–220. http://doi.org/10.1016/j.jcis.2014.05.036

Antonov, M., Mazzawi, M., & Dubin, P. L. (2010). Entering and Exiting the Protein−Polyelectrolyte Coacervate Phase via Nonmonotonic Salt Dependence of Critical Conditions. *Biomacromolecules*, *11*(1), 51–59. http://doi.org/10.1021/bm900886k

Burgess, D. J., & Carless, J. E. (1984). Microelectrophoretic studies of gelatin and acacia for the prediction of complex coacervation. *Journal of Colloid and Interface Science*, *98*(1), 1–8. http://doi.org/10.1016/0021-9797(84)90472-7

Chapeau, A.-L., Tavares, G. M., Hamon, P., Croguennec, T., Poncelet, D., & Bouhallab, S. (2016). Spontaneous co-assembly of lactoferrin and β-lactoglobulin as a promising biocarrier for vitamin B9. *Food Hydrocolloids*, *57*, 280–290. http://doi.org/10.1016/j.foodhyd.2016.02.003

Comert, F., & Dubin, P. L. (2017). Liquid-liquid and liquid-solid phase separation in protein-polyelectrolyte systems. *Advances in Colloid and Interface Science*, *239*, 213–217. http://doi.org/10.1016/J.CIS.2016.08.005

Comert, F., Malanowski, A. J., Azarikia, F., & Dubin, P. L. (2016). Coacervation and precipitation in polysaccharide-protein systems. *Soft Matter*, *12*(18), 4154–61. http://doi.org/10.1039/c6sm00044d

Cousin, F., Gummel, J., Combet, S., & Boué, F. (2011). The model Lysozyme–PSSNa system for electrostatic complexation: Similarities and differences with complex coacervation. *Advances in Colloid and Interface Science*, *167*(1–2), 71–84. http://doi.org/10.1016/J.CIS.2011.05.007

de Kruif, C. G., Weinbreck, F., & de Vries, R. (2004). Complex coacervation of proteins and anionic polysaccharides. *Current Opinion in Colloid & Interface Science*, *9*(5), 340–349. http://doi.org/10.1016/J.COCIS.2004.09.006

Ericson, M. L., Rödin, J., Lenman, M., Glimelius, K., Josefsson, L. G., & Rask, L. (1986). Structure of the rapeseed 1.7 S storage protein, napin, and its precursor. *The Journal of Biological Chemistry*, *261*(31), 14576–81. http://www.ncbi.nlm.nih.gov/pubmed/3771543

Gehrig, P. M., Krzyzaniak, A., Barciszewski, J., & Biemann, K. (1996). Mass spectrometric amino acid sequencing of a mixture of seed storage proteins (napin) from Brassica napus, products of a multigene family. *Proceedings of the National Academy of Sciences of the United States of America*, *93*(8), 3647–52. http://www.ncbi.nlm.nih.gov/pubmed/8622990

Josefsson, L. G., Lenman, M., Ericson, M. L., & Rask, L. (1987). Structure of a gene encoding the 1.7 S storage protein, napin, from Brassica napus. *The Journal of Biological Chemistry*, *262*(25), 12196–201. http://www.ncbi.nlm.nih.gov/pubmed/3624251

Kizilay, E., Kayitmazer, A. B., & Dubin, P. L. (2011). Complexation and coacervation of polyelectrolytes with oppositely charged colloids. *Advances in Colloid and Interface Science*, *167*(1), 24–37. http://doi.org/10.1016/j.cis.2011.06.006

Mattison, K. W., Brittain, I. J., & Dubin, P. L. (1995). Protein-Polyelectrolyte Phase Boundaries. *Biotechnology Progress*, *11*(6), 632–637. http://doi.org/10.1021/bp00036a005

Mattison, K. W., Dubin, P. L., & Brittain, I. J. (1998). Complex Formation between Bovine Serum Albumin and Strong Polyelectrolytes: Effect of Polymer Charge Density. *The Journal of Physical Chemistry B*, *102*(19), 3830–3836. http://doi.org/10.1021/jp980486u

McMullen, J. N., Newton, D. W., & Becker, C. H. (1982). Pectin-gelatin complex coacervates I: Determinants of microglobule size, morphology, and recovery as water-dispersible powders. *Journal of Pharmaceutical Sciences*, *71*(6), 628–33. http://www.ncbi.nlm.nih.gov/pubmed/7097523

Monsalve, R. I., & Rodriguez, R. (1990). *Purification and Characterization of Proteins from the 2S Fraction from Seeds of the Brassicaceae Family*. *Journal of Experimental Botany*, 41(222), 89-94. http://doi.10.1093/jxb/41.1.89

Mosse, J. (1990). Nitrogen-to-protein conversion factor for ten cereals and six legumes or oilseeds. A reappraisal of its definition and determination. Variation according to species and to seed protein content. *Journal of Agricultural and Food Chemistry*, *38*(1), 18–24. http://doi.org/10.1021/jf00091a004

Nigen, M., Croguennec, T., Renard, D., & Bouhallab, S. (2007). Temperature Affects the Supramolecular Structures Resulting from α-Lactalbumin−Lysozyme Interaction. *Biochemistry*,

46(5), 1248-1255. http://doi.org/10.1021/BI062129C

Niu, F.G., Su, Y.J., Liu, Y.T., Wang, G.C., Zhang, Y., & Yang, Y.Y. (2014). Ovalbumin-gum arabic interactions: Effect of pH, temperature, salt, biopolymers ratio and total concentration. *Colloids and Surfaces B-Biointerfaces*, 113, 477-482. http://doi. 10.1016/j.colsurfb.2013.08.012

Niu, F.G., Dong, Y.T., Shen, F., Wang, J.Q., Liu, Y.T., Su, Y.J., Xu, R.R., Wang, J.W., & Yang, Y.J. (2015). Phase separation behavior and structural analysis of ovalbumin-gum arabic complex coacervation. *Food Hydrocolloids*, 43, 1-7. http://doi. 10.1016/j.foodhyd.2014.02.009

Obermeyer, A. C., Mills, C. E., Dong, X.-H., Flores, R. J., & Olsen, B. D. (2016). Complex coacervation of supercharged proteins with polyelectrolytes. *Soft Matter*, *12*(15), 3570–3581. http://doi.org/10.1039/C6SM00002A

Pathak, J., Priyadarshini, E., Rawat, K., & Bohidar, H.B. (2017). Complex coacervation in charge complementary biopolymers: Electrostatic versus surface patch binding. *Advances in Colloid and Interface Scienc*e, 250, 40-53. http://doi. 10.1016/j.cis.2017.10.006

Ralet, M.-C., Dronnet, V., Buchholt, H. C., & Thibault, J.-F. (2001). Enzymatically and chemically de-esterified lime pectins: characterisation, polyelectrolyte behaviour and calcium binding properties. *Carbohydrate Research*, *336*(2), 117–125. http://doi.org/10.1016/S0008-6215(01)00248-8

Renard, D., Lavenant-Gourgeon, L., Ralet, M., & Sanchez, C. (2006). Acacia senegal Gum: Continuum of Molecular Species Differing by Their Protein to Sugar Ratio, Molecular Weight, and Charges. Biomacromolecules, 7(9), 2637–2649.

Rico, M., Bruix, M., González, C., Monsalve, R. I., & Rodríguez, R. (1996). 1H NMR assignment and global fold of napin BnIb, a representative 2S albumin seed protein. Biochemistry, 35(49), 15672–15682.

Romanini, D., Braia, M., Angarten, R. G., Loh, W., & Picó, G. (2007). Interaction of lysozyme with negatively charged flexible chain polymers. *Journal of Chromatography B*, *857*(1), 25–31. http://doi.org/10.1016/J.JCHROMB.2007.06.025

Salis, A., Boström, M., Medda, L., Cugia, F., Barse, B., Parsons, D. F., Ninham, B.W., & Monduzzi, M. (2011). Measurements and Theoretical Interpretation of Points of Zero Charge/Potential of BSA Protein. *Langmuir*, *27*(18), 11597–11604. http://doi.org/10.1021/la2024605

Sanchez, C., Mekhloufi, G., Schmitt, C., Renard, D., Robert, P., Lehr, C.M., Lamprecht, A., & Hardy, J. (2002). Self-assembly of beta-lactoglobulin and acacia gum in aqueous solvent: Structure and

phase-ordering kinetics. *Langmuir*, 18(26), 10323-10333. http://doi.10.1021/la0262405

Sanchez, C., Lapp, A., Schmitt, C., Gaillard, C., Kolodziejczyk, E., & Renard, D. (2008). The Acacia gum arabinogalactan fraction is a thin oblate ellipsoid: a new model based on SANS and *ab initio* calculation, *Biophysical Journal*, 94, 629-639

Schmidt, I. (2004). *Structures et propriétés tensioactives des assemblages complexes protéines basiques/pectines*. PhD Thesis, Université de Nantes. France.

Schmidt, I., Renard, D., Rondeau, D., Richomme, P., Popineau, Y., & Axelos, M. A.-V. (2004). Detailed Physicochemical Characterization of the 2S Storage Protein from Rape (*Brassica napus* L.). *Journal of Agricultural and Food Chemistry*, *52*(19), 5995–6001. http://doi.org/10.1021/jf0307954

Schmidt, I., Cousin, F., Huchon, C., Boué, F., & Axelos, M. A. V. (2009). Spatial Structure and Composition of Polysaccharide−Protein Complexes from Small Angle Neutron Scattering. *Biomacromolecules*, *10*(6), 1346–1357.

Schmitt, C., & Turgeon, S. L. (2011). Protein/polysaccharide complexes and coacervates in food systems. *Advances in Colloid and Interface Science*, *167*(1), 63–70. http://doi.org/10.1016/j.cis.2010.10.001

Schmitt, C., Sanchez, C., Thomas, F. & Hardy, J. (1999). Complex coacervation between beta-lactoglobulin and acacia gum in aqueous medium. *Food Hydrocolloids*, 13(6), 483-496. http://doi.10.1016/S0268-005X(99)00032-6

Song, H., Tice, J. D., & Ismagilov, R. F. (2003). A Microfluidic System for Controlling Reaction Networks in Time. *Angewandte Chemie International Edition*, *42*(7), 768–772. http://doi.org/10.1002/anie.200390203

Sperber, B.L.H.M., Schols, H.A., Stuart, M.A.C., Norde, W.? & Voragen, A.G.J. (2009). Influence of the overall charge and local charge density of pectin on the complex formation between pectin and beta-lactoglobuli. *Food Hydrocolloids*, 23(3), 765-772. http://doi. 10.1016/j.foodhyd.2008.04.008

Tavares, G. M., Croguennec, T., Hamon, P., Carvalho, A. F., & Bouhallab, S. (2015). Selective coacervation between lactoferrin and the two isoforms of β-lactoglobulin. *Food Hydrocolloids*, *48*, 238–247. http://doi.org/10.1016/j.foodhyd.2015.02.027

Thibault, J. F. (1979). Automatisation du dosage des substances pectiques par la methode au meta-hydroxydiphenyl. *Lebensmittel - Wissenschaft + Technologie. Food Science + Technology*.

http://agris.fao.org/agris-search/search.do?recordID=US201302848114

Thongkaew, C., Hinrichs, J., Gibis, M., & Weiss, J. (2015). Sequential modulation of pH and ionic strength in phase separated whey protein isolate – Pectin dispersions: Effect on structural organization. *Food Hydrocolloids*, *47*, 21–31. http://doi.org/10.1016/J.FOODHYD.2014.11.006

Tiwari, A., Bindal, S., & Bohidar, H. B. (2009). Kinetics of Protein−Protein Complex Coacervation and Biphasic Release of Salbutamol Sulfate from Coacervate Matrix. *Biomacromolecules*, *10*(1), 184–189. http://doi.org/10.1021/bm801160s

Turgeon, S. L., Schmitt, C., & Sanchez, C. (2007). Protein–polysaccharide complexes and coacervates. *Current Opinion in Colloid & Interface Science*, *12*(4–5), 166–178. http://doi.org/10.1016/J.COCIS.2007.07.007

Veis, A., Bodor, E., & Mussell, S. (1967). Molecular weight fractionation and the self-suppression of complex coacervation. *Biopolymers*, *5*(1), 37–59. http://doi.org/10.1002/bip.1967.360050106

Vinayahan, T., Williams, P.A., & Phillips, G.O. (2010). Electrostatic interaction and complex formation between gum arabic and bovine serum albumin. *Biomacromolecules*, 11(12), 3367-3374. http://doi. 10.1021/bm100486p

Wee, M.S.M., Nurhazwani, S., Tan, K.W.J., Goh, K.K.T., Sims, I.M., & Matia-Merino, L. (2014). Complex coacervation of an arabinogalactan-proteinextracetd from the Meryta sinclarii tree (puka gum) and whey protein isolate. *Food Hydrocolloids*, 42, 130-138, Part: 1 Special issue SI. http://doi. 10.1016/j.foodhyd.2014.03.005

Xia, J., & Dubin, P. L. (1994). Protein-Polyelectrolyte Complexes. In *Macromolecular Complexes in Chemistry and Biology* (pp. 247–271). Berlin, Heidelberg: Springer Berlin Heidelberg. http://doi.org/10.1007/978-3-642-78469-9_15

Zaitsev, V., Izumrudov, V., & Zezin, A. (1992). New type of water-soluble protein-polyelectrolyte complexes. *VYSOKOMOLEKULYARNYE SOEDINENIYA SERIYA A*, 34(1), 138–139.

Figure captions

Figure 1. Droplets-based millifluidic for the screening of biopolymers interactions A. Droplets-based millifluidic experimental set-up B. Millifluidic droplets production using a co-flow geometry. Mixing between napin (NAP) and pectin (PEC) biopolymers was ensured by a T-junction using sunflower oil (OIL) as continuous phase. C. Droplets flowed through a winding tube to optimize the mixing within droplets based on chaotic advection. D. Polydimethylsiloxane (PDMS) bath designed for droplets observation and limitation of reflexion. Observations were performed using a camera and an objective to get dark field images. E. Detachable module used for long term storage of 9 mixing conditions. Flow was guided in the desired tube using slide clamps.

Figure 2. Electrophoretic mobility of napin (cicrcles) and pectin (squares) as a function of pH. Measurements were performed in triplicates at 0.25 wt% in water. Dashed and dotted lines are guide to the eye.

Figure 3. Turbidity of NAP/PEC mixtures as a function of the initial mixing ratios at pH 4, 5, 6 and 7 at a total biopolymers concentration of 0.1 wt% and I = 25 mM.

Figure 4. Impact of biopolymers total concentration (from 0.1 to 1 wt%) at pH 4 on NAP/PEC interactions investigated through droplets-based millifluidic. A. Evolution of the droplet grey level as a function of mixing ratio and total concentration. B. Examples of millifluidic droplets observed on-line containing NAP/PEC mixtures at various mixing ratio and total concentration. C. NAP/PEC phase diagram obtained from droplets-based millifluidic experiments and highlighting monophasic (empty circles) and biphasic conditions (filled circles). D. Phase separation yield (%) as a function of mixing ratio at pH 4 and total biopolymer concentration of 0.5 wt%.

Figure 5. Phase contrast microscopy observations in time of NAP/PEC mixtures at a total biopolymer concentration of 0.5 wt%, pH 4, I = 25mM and mixing ratios of 8:1, 4:1, 3:2, 1:1 and 2:3.

Figure 6. Evolution of the electrophoretic mobility of NAP/PEC mixtures prepared at various mixing ratio. Experiments were conducted at I = 25 mM, pH = 4 and 0.5 wt% total biopolymer concentration.

Figure 7. A. Surface charge density Z_p/M_w of biopolymers obtained by potentiometric titration of 0.1wt% biopolymers dispersions in water. B. Evolution of Pr/Ps charge ratio in the initial mixture and in the lower dense phase as a function of the initial napin concentration. Pr/Ps charge ratios were obtained from potentiometric titrations and phase compositions at thermodynamic equilibrium. Red dashed line represents a Pr/Ps charge ratio equal to 1.

Figure 8. Structures obtained by phase contrast microscopy for a Pr:Ps weight mixing ratio of 8:1 at pH 4, 5, and 9. Total biopolymers concentration was set at 0.5 wt% and I = 25 mM.

Figure 9. A. Turbidity measured at 600 nm of Napin/HIC-F1 mixtures as a function of napin content at a total biopolymer concentration of 0.5 wt% in 25 mM acetate buffer (pH = 4.0, I = 25 mM). B. Phase contrast microscopy of Napin/ HIC-F1 mixtures for mixing ratio of 8:1, 4:1, 3:2 and 2:3. Scale bars stand for 50 µm.

Figure 10. A. 3D-structure of Napin resolved by NMR (Rico, Bruix, González, Monsalve, & Rodríguez, 1996) Arrows indicate disordered loops. B. Hydropathy index calculated using Expasy Webserver according to Kyle & Doolittle. In blue, the two polypeptide chains linked by disulphide bonds in native napin are reported. In blue, disordered domains are reported.

Figure 1

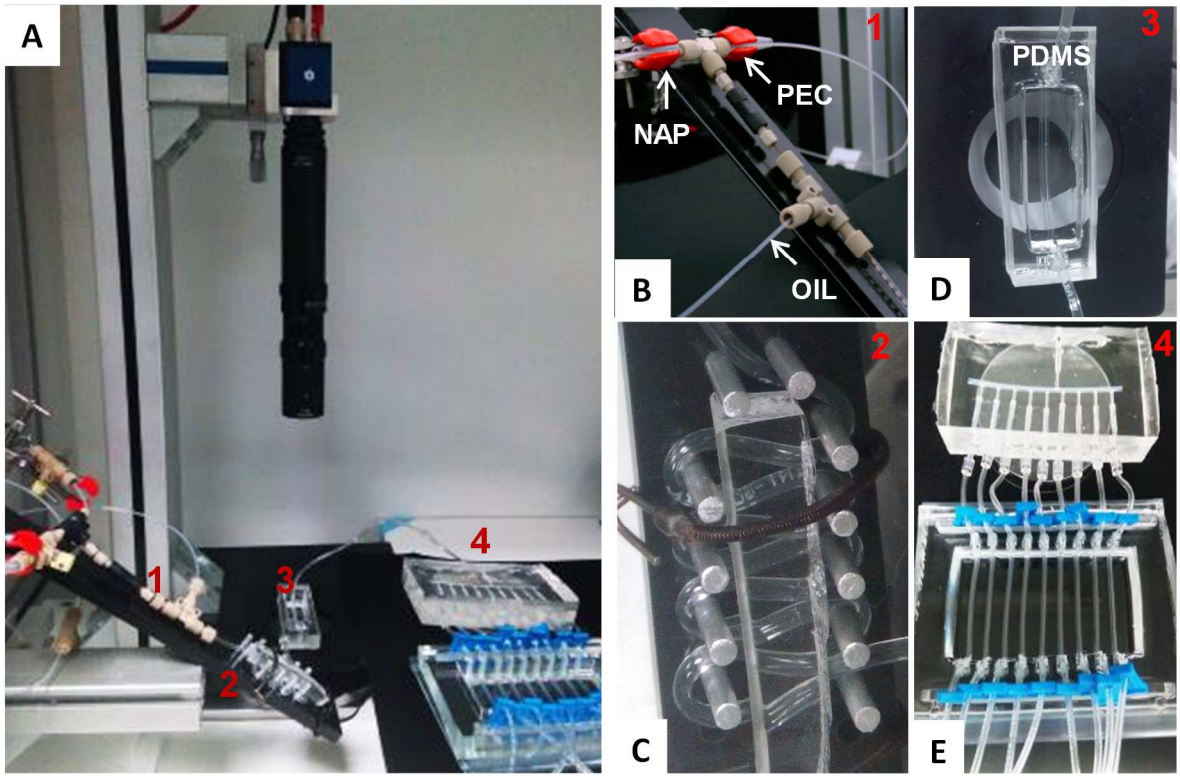

Figure 2

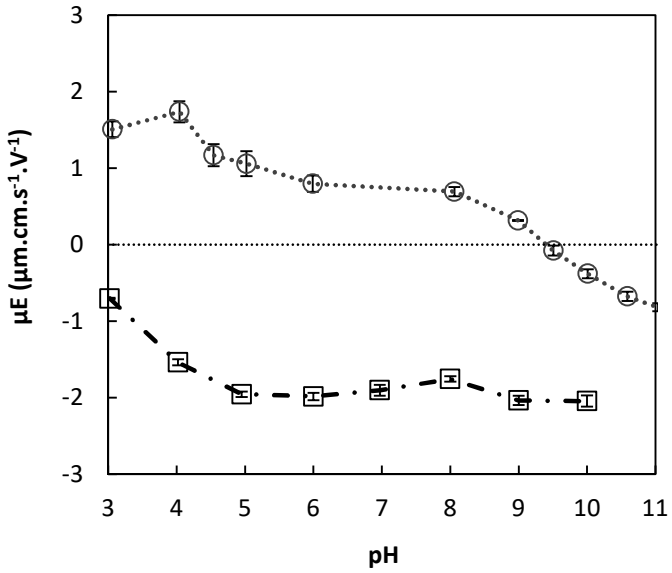

Figure 3

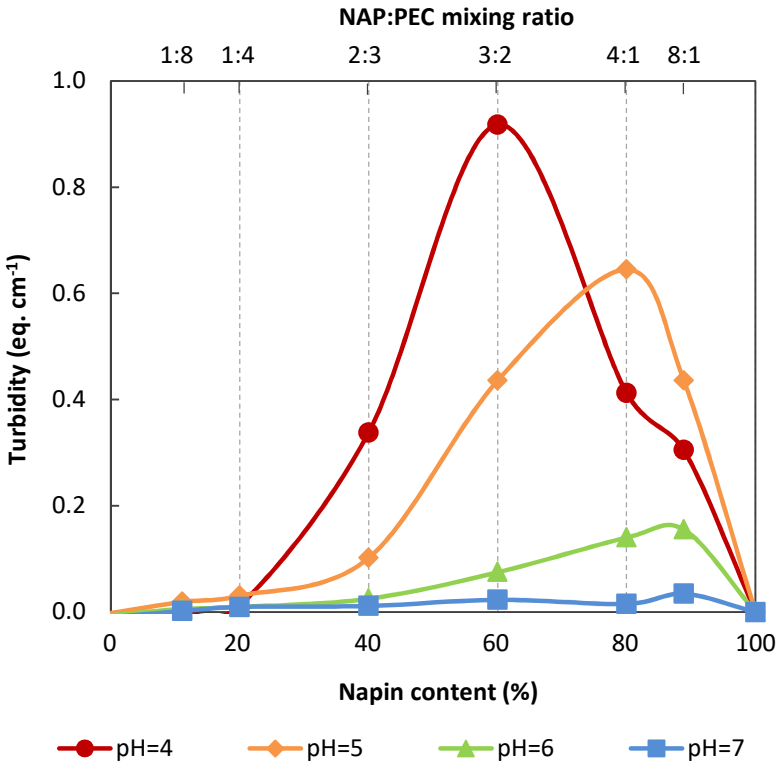
NAP:PEC mixing ratio
1:8
1:4
2:3
3:2
4:1
8:1
1.0
0.8
0.6
0.4
0.2
0.0
Turbidity (eq. cm-1)
0
20
40
60
80
100
Napin content (%)
pH=4
pH=5
pH=6
pH=7

Figure 4

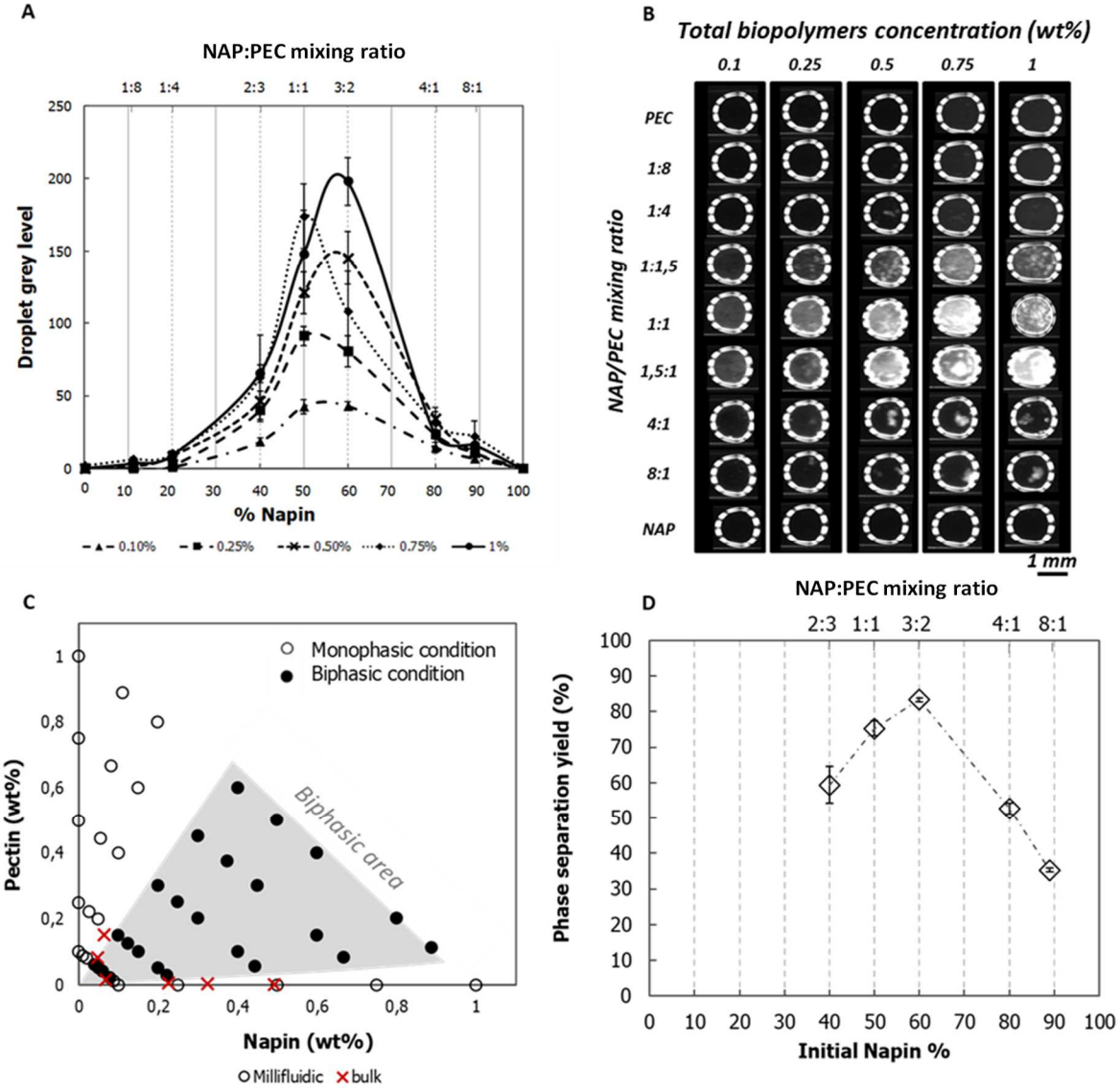
A
NAP:PEC mixing ratio
1:8 1:4 2:3 1:1 3:2 4:1 8:1
Droplet grey level
% Napin
0.10% 0.25% 0.50% 0.75% 1%
B
Total biopolymers concentration (wt%)
0.1 0.25 0.5 0.75 1
NAP/PEC mixing ratio
PEC
1:8
1:4
1:1,5
1:1
1,5:1
4:1
8:1
NAP
1 mm
C
Monophasic condition
Biphasic condition
Biphasic area
Pectin (wt%)
Napin (wt%)
Millifluidic
bulk
D
NAP:PEC mixing ratio
2:3 1:1 3:2 4:1 8:1
Phase separation yield (%)
Initial Napin %

Figure 5

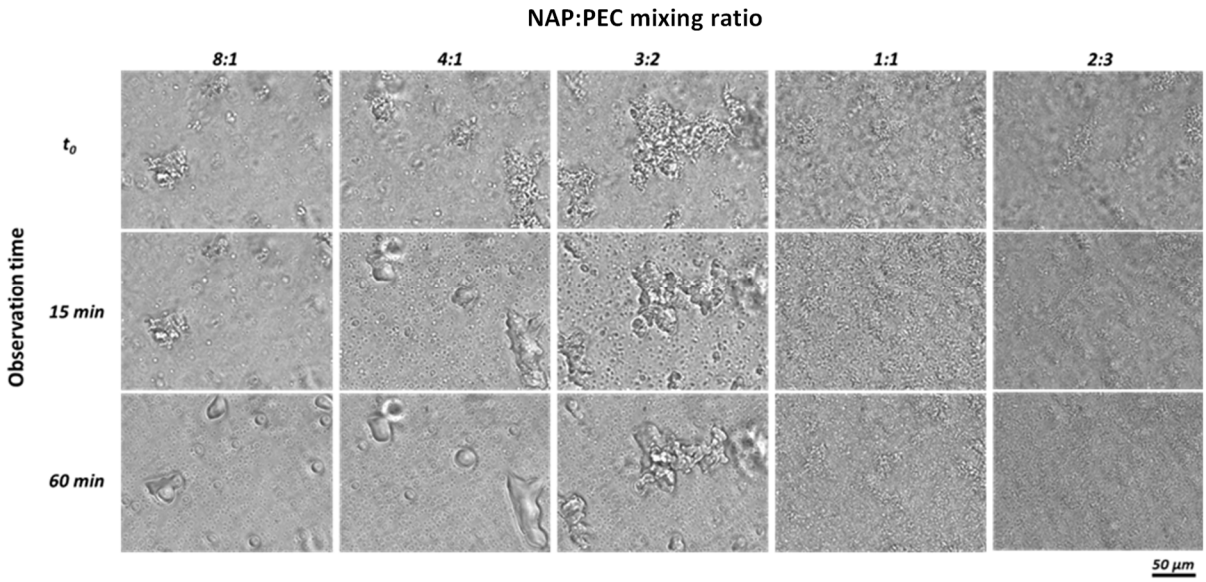
NAP:PEC mixing ratio
8:1
4:1
3:2
1:1
2:3
Observation time
t_0
15 min
60 min
50 µm

Figure 6

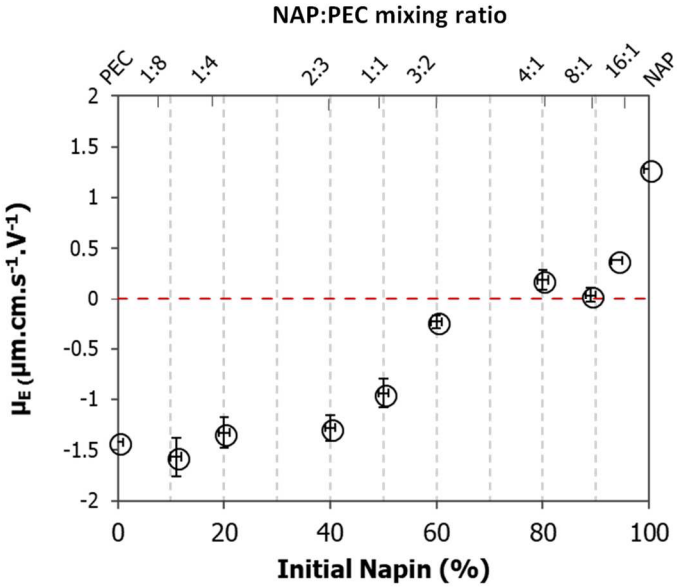
NAP:PEC mixing ratio
PEC
1:8
1:4
2:3
1:1
3:2
4:1
8:1
16:1
NAP
2
1.5
1
0.5
0
-0.5
-1
-1.5
-2
0
20
40
60
80
100
Initial Napin (%)
μE (μm.cm.s-1.V-1)

Figure 7

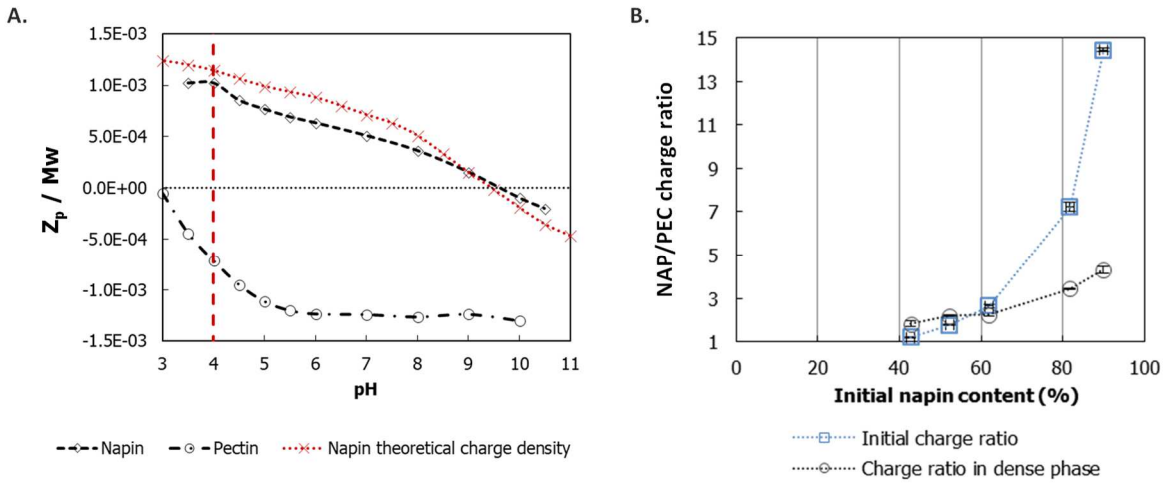
A.
1.5E-03
1.0E-03
5.0E-04
0.0E+00
-5.0E-04
-1.0E-03
-1.5E-03
Z_p / Mw
3
4
5
6
7
8
9
10
11
pH
Napin
Pectin
Napin theoretical charge density
B.
15
13
11
9
7
5
3
1
NAP/PEC charge ratio
0
20
40
60
80
100
Initial napin content (%)
Initial charge ratio
Charge ratio in dense phase

Figure 8

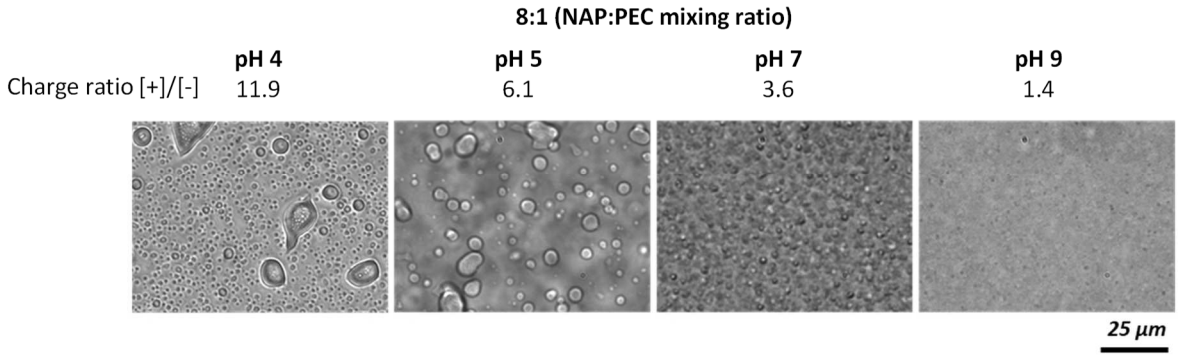
8:1 (NAP:PEC mixing ratio)
pH 4
pH 5
pH 7
pH 9
Charge ratio [+]/[-]
11.9
6.1
3.6
1.4
25 µm

Figure 9

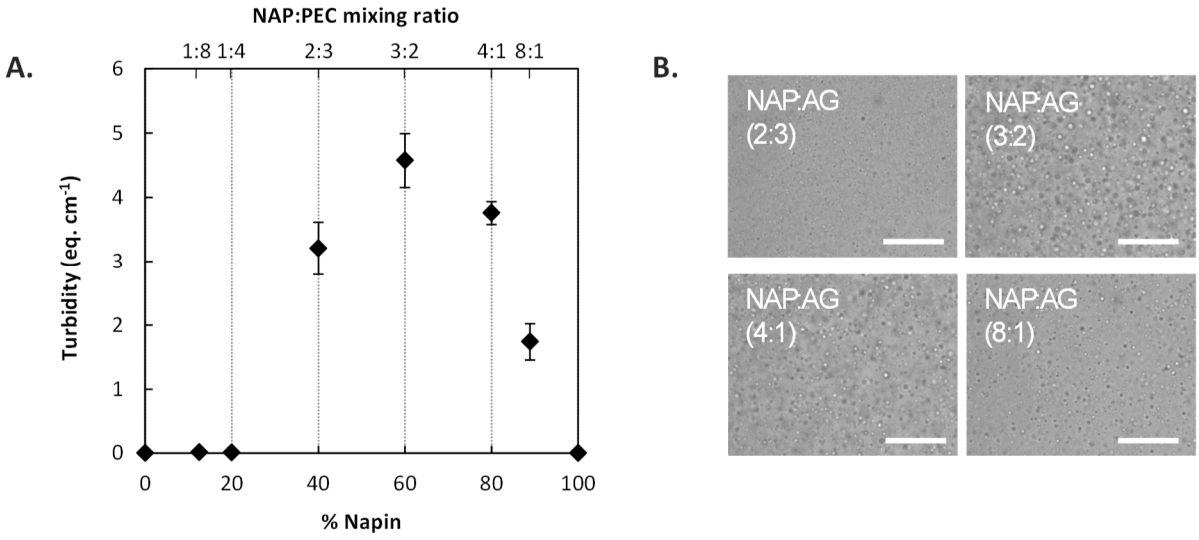
A.
NAP:PEC mixing ratio
1:8 1:4 2:3 3:2 4:1 8:1
Turbidity (eq. cm-1)
0 1 2 3 4 5 6
0 20 40 60 80 100
% Napin
B.
NAP:AG (2:3)
NAP:AG (3:2)
NAP:AG (4:1)
NAP:AG (8:1)

Figure 10

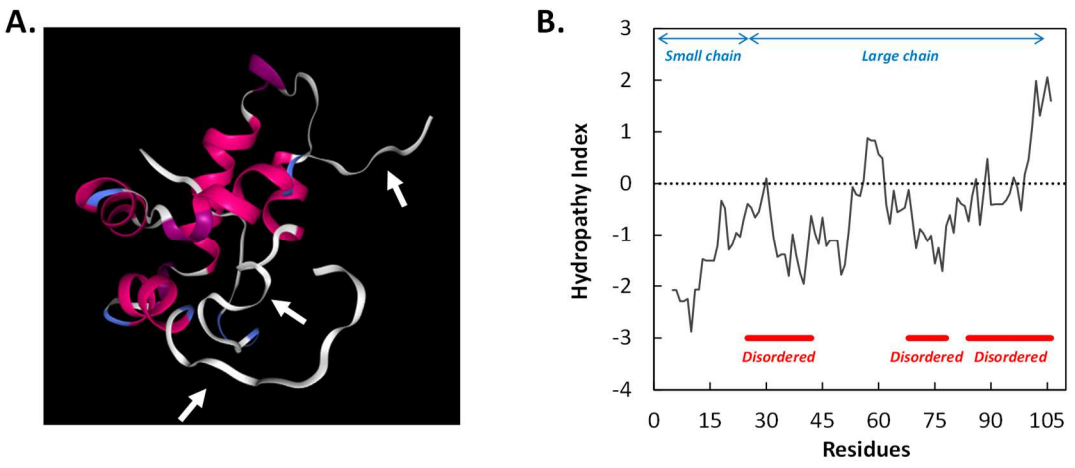
A.
B.
Small chain
Large chain
Hydropathy Index
3
2
1
0
-1
-2
-3
-4
Disordered
Disordered
Disordered
0
15
30
45
60
75
90
105
Residues

Table 1. Equivalence between protein:polysaccharide (Pr:Ps) ratio and proportion of napin (NAP) (%) in the initial mixture

Pr:Ps mass ratio	**0:1**	**1:8**	**1:4**	**2 :3**	**1:1**	**3 :2**	**4:1**	**8:1**	**1:0**
% of NAP in initial mixture	0	11	20	40	50	60	80	89	100

Graphical abstract